(12)

(15) N00014-76-C-0547

DDC
RECEIVED
SEP 27

(6)

CONTACT STRESS ANALYSIS OF CERAMIC-TO-METAL INTERFACES, FINAL REPORT.

(14) 21-3239 (11) 22 September 21, 1979 (13) 35 p.

(12) David G. Finger

Prepared by Engineering Staff/WRB

Initial Issue Approved by

G. F. Austin, Program Manager, Advanced Technology

David G. Finger

D. G. Finger, Principal Investigator, Mechanical Component Design, Engineering Sciences

AIRESEARCH MANUFACTURING COMPANY
A DIVISION OF THE GARRETT CORPORATION
PHOENIX, ARIZONA

REPORT NO. 21-3239

TOTAL PAGES 32

ATTACHMENTS:

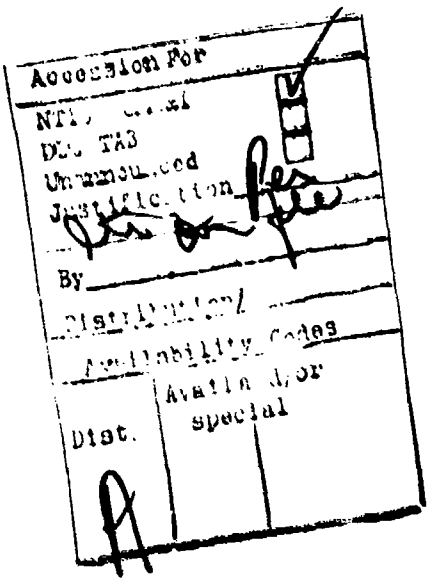

REV	BY	APPROVED	DATE	PAGES AND/OR PARAGRAPHS AFFECTED

AIRESEARCH MANUFACTURING COMPANY OF ARIZONA
A DIVISION OF THE GARRETT CORPORATION
PHOENIX, ARIZONA

CONTRACT STRESS ANALYSIS OF CERAMIC-TO-METAL INTERFACES FINAL REPORT

1.0 INTRODUCTION

This Final Report presents the technical progress completed for Contract N00014-78-C-0547, "Contact Stress Analysis of Ceramic-to-Metal Interfaces."

The Navy Scientific Officer is Mr. Bob Pohanka.

The objective of this proposed 8-month program was to conduct analysis, specimen testing, and data correlation to provide an improved understanding of the local contact conditions that prevail at an interface between ceramic and metal components for gas turbine engines. The program was specifically directed to study contact stresses at the interface between inserted ceramic turbine blades (hot-pressed silicon nitride) and a metal rotor, but the method of analysis, results, and conclusions also provided a better understanding of contact stresses at ceramic-to-metal and ceramic-to-ceramic interfaces for static components.

A finite-element stress analysis procedure and structural evaluation technique consistent with the statistical nature of ceramic materials was generated. Specimen testing was conducted to obtain validation of these techniques and provide insight as to possible modifications of stress simulation or fracture prediction criteria. The objective was to develop a design methodology, which will improve on current design methods, thus permitting the design of interface configurations in which strengths more indicative of the inherent strength of ceramic materials can be realized.

This four-task effort was subdivided as follows:

AIRESEARCH MANUFACTURING COMPANY OF ARIZONA
A DIVISION OF THE GARRETT CORPORATION
PHOENIX, ARIZONA

Task I Boundary Condition Study

Task II Finite-Element Model Development and Analysis

Task III Specimen Testing and Model Validation

Task IV Reporting

2.0 TECHNICAL PROGRESS SUMMARY

Task I of the program, Boundary Condition Study, has been completed. A simplified model, a cylinder on a plane, was devised which could be analyzed with both a closed-form solution and a finite-element computer program. This model is also amenable to specimen testing.

Task II of the program, Finite-Element Model Development and Analysis, has been completed. Significant progress has been made in modeling the contact zone of the ceramic-to-metal interface region. A cylinder in contact with a plane was chosen for the analytical approach because it not only approximates the situation of ceramic blade to rotor attachments, but it provides closed-form and finite-element solutions for both the non-friction and friction cases.

Task III, Specimen Testing and Model Validation, has been completed. A test fixture for the verification testing has been designed and fabricated to apply a tensile load to the ceramic specimens while applying a compressive normal contact load. Various ratios between compressive and tensile loads have been investigated with and without compliant layers. Both HS25 and platinum compliant material have been investigated.

Task IV, Reporting, has been completed with the submission of the Final Report, which documents the work completed within this 8-month program.

2.1 Analytical Approach and Accomplishments

Zoom finite-element modeling techniques have been used successfully to calculate stresses in the interface between bodies in contact. Good agreement has been achieved between closed-form solutions, References 1 and 2, and finite-element models for a cylinder contacting a semi-infinite solid with and without friction forces. These

particular solutions approximate a ceramic blade-to-metallic disk attachment.

As previously reported, a finite-element approach was used to analyze the frictionless case for a ceramic cylinder and a ceramic plate. The analysis employed zoom modeling to provide a sufficient number of nodes in the region of contact. The original model, Figure 1, provided boundary conditions for a more refined model of the contact zone, Figure 2. This model did not have sufficient refinement to give adequate representation of the contact zone. Consequently, results for this model provided input for a more refined finite-element mesh. As before, this refined model still did not have sufficient nodes in the interface region to completely depict the stress distribution, so a final zoom model was generated which had thirteen nodes in the contact zone, Figure 3. The relative sizes of the four finite-element models are shown in Figure 4. Figure 5 compares the stresses in the direction normal to the plane for the four finite-element models and a classical closed-form solution from Reference 1. Good agreement was also achieved for maximum shear stresses and transverse stresses.

Contact between dissimilar materials was also studied. An analysis similar to that mentioned above was completed for an aluminum cylinder, $E = 7.10 \times 10^6$ N/cm^2, and a ceramic plate, $E = 28.96 \times 10^7$ N/cm^2. Results from the zoom finite-element solution agreed well with the closed-form results, Figure 6.

The transverse and shear stress distributions change considerably when friction forces are included. The addition of friction effects appears to be the key in understanding the stress distribution in contact interfaces between ceramic and metal components, especially blade/disk interfaces. Therefore, classical solutions for bodies in contact with both normal and tangential loads were examined. Figure 7 shows the tangential stresses for various ratios between the normal

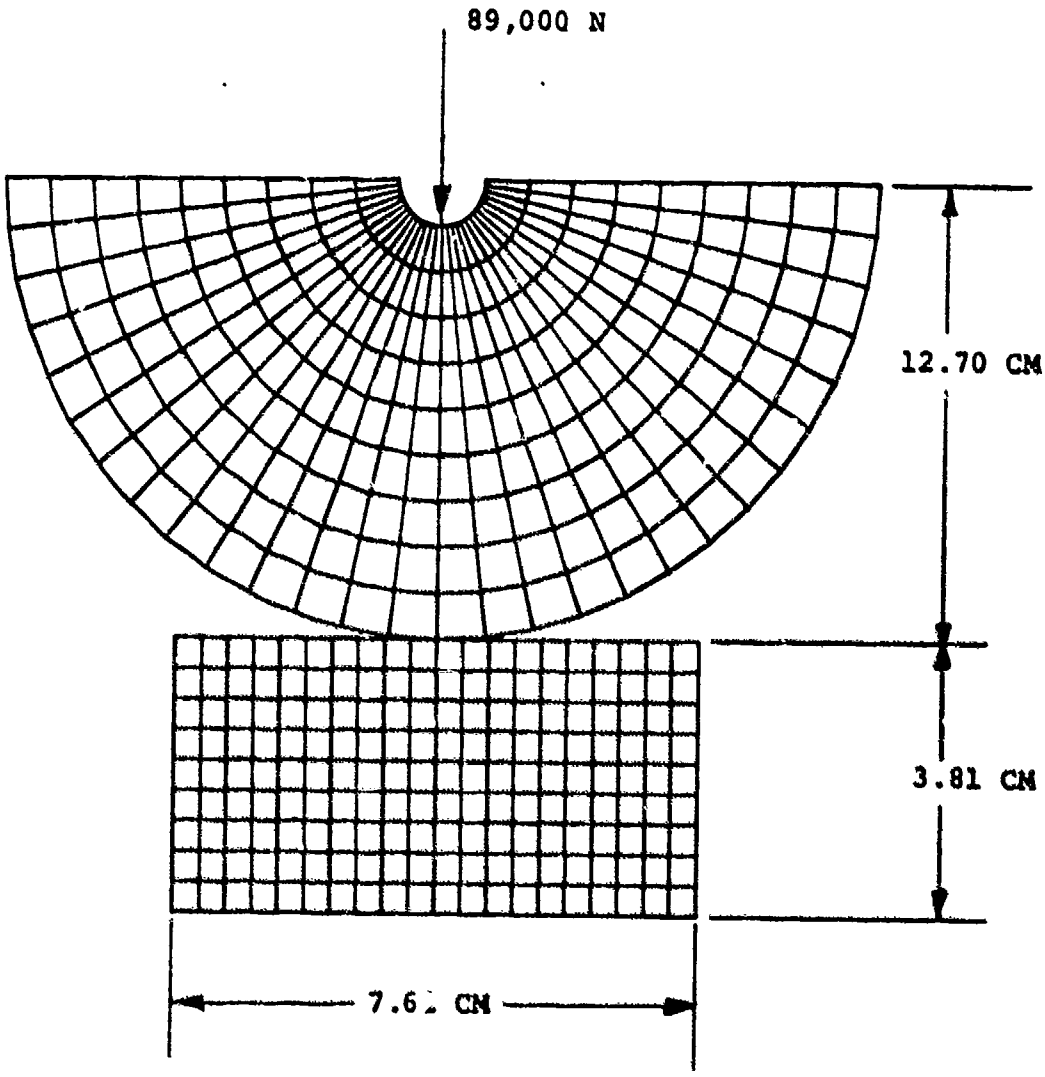

Figure 1. Original Finite-Element Model.

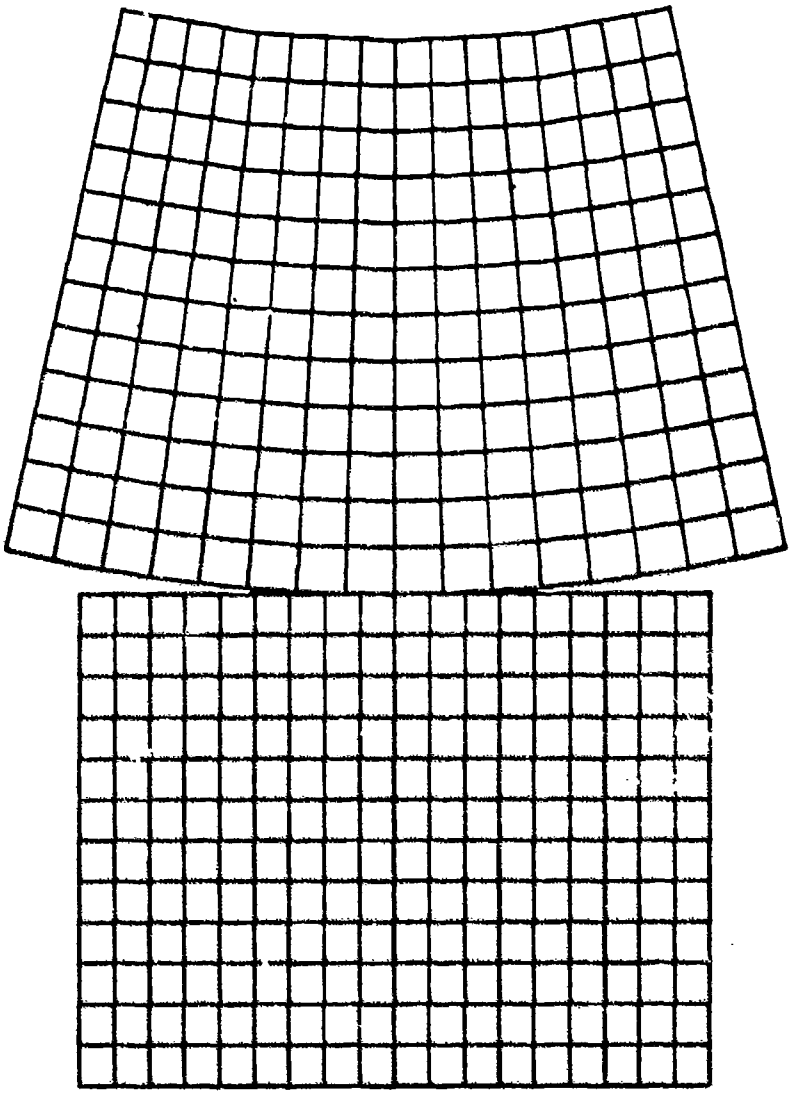

Figure 2. Refined Finite-Element Model.

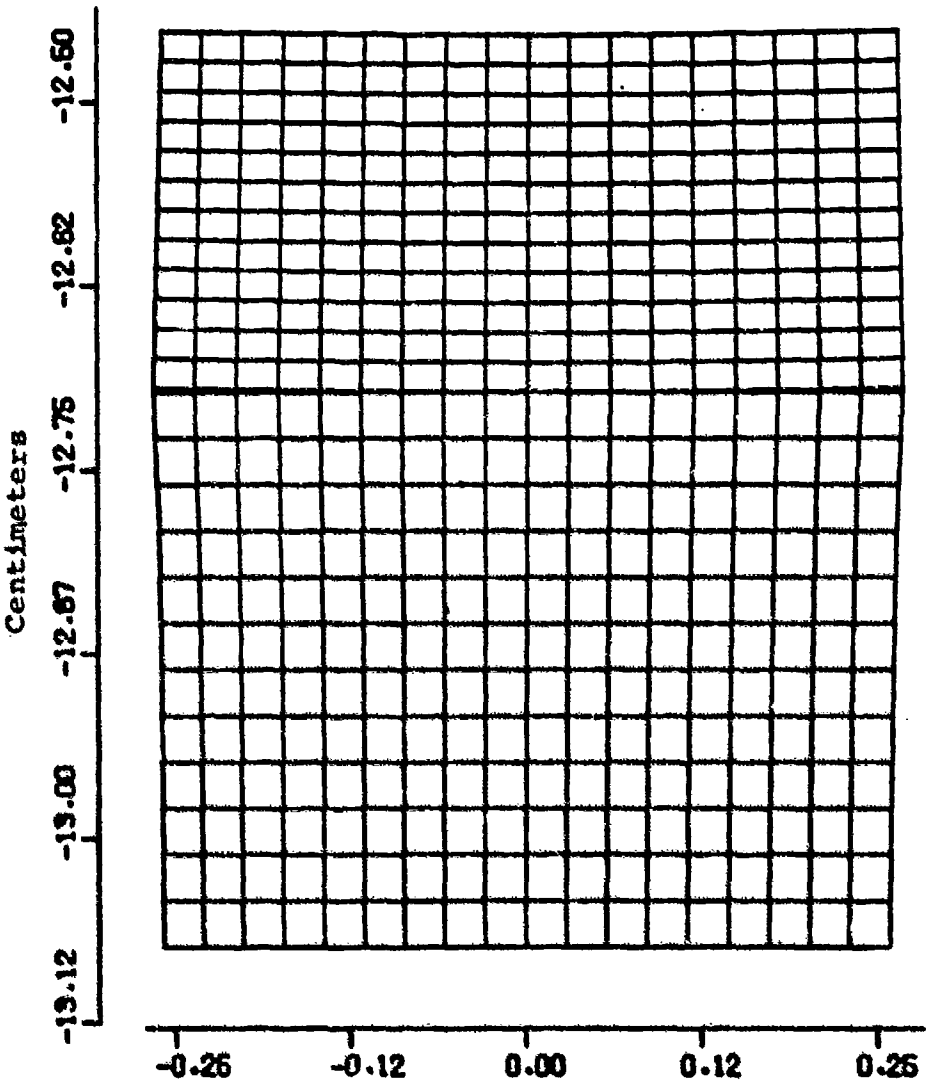

Figure 3. Final Zoom Finite-Element Model.

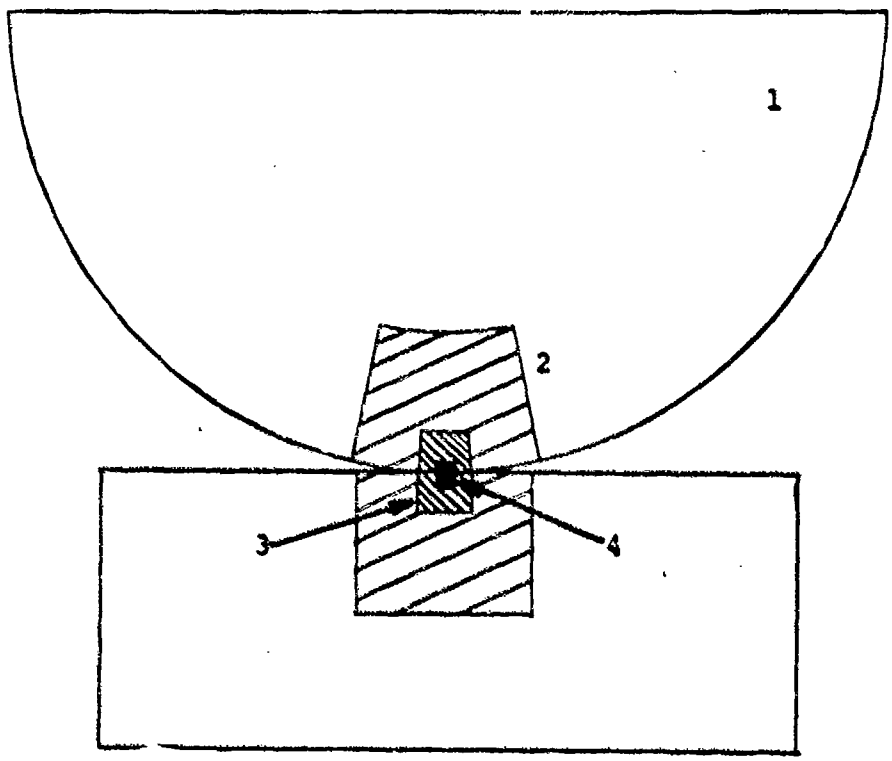

Figure 4. Relative Size of Finite-Element Model.

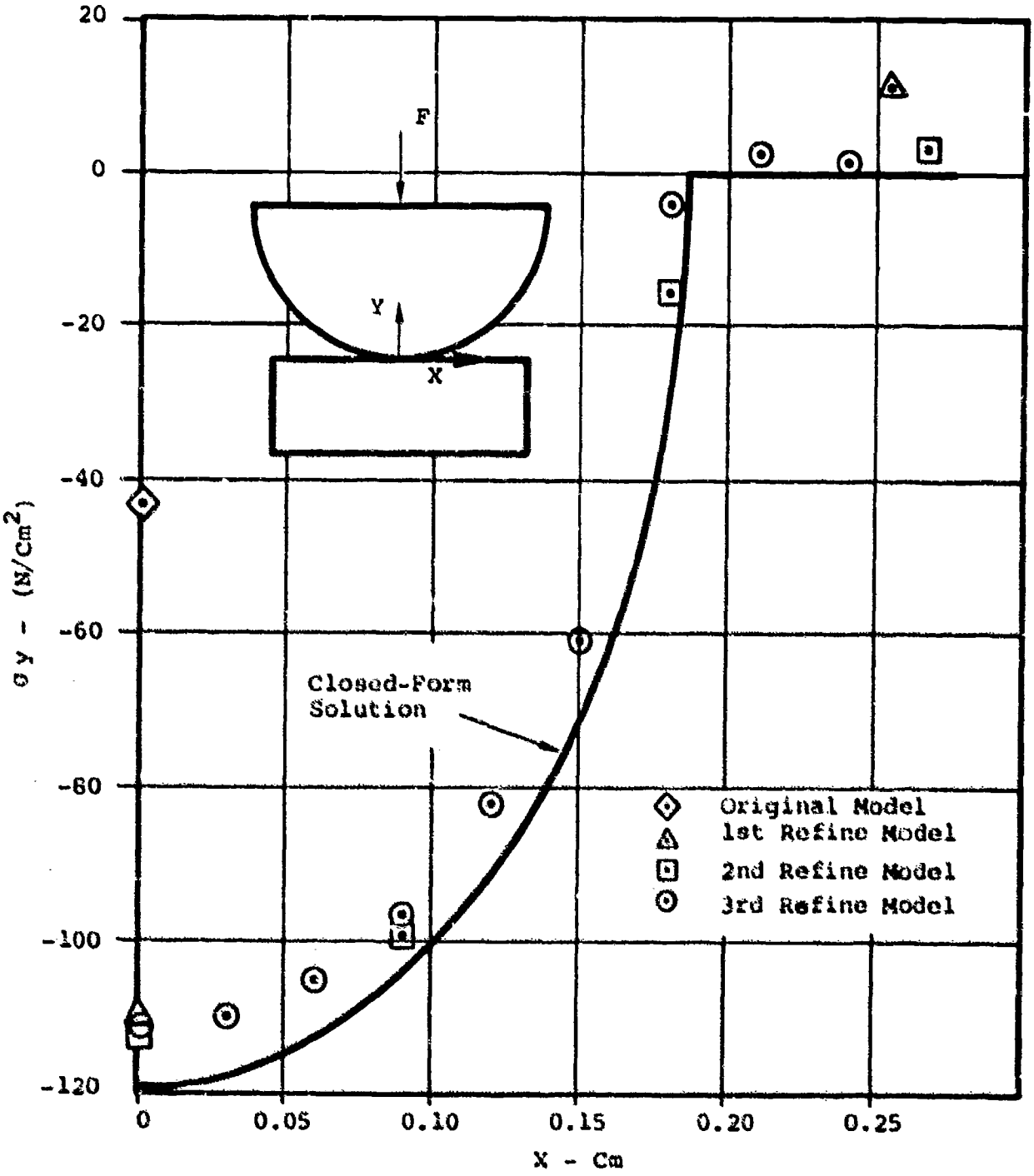

Figure 5. Comparison of Finite Element to Closed-Form Solution.

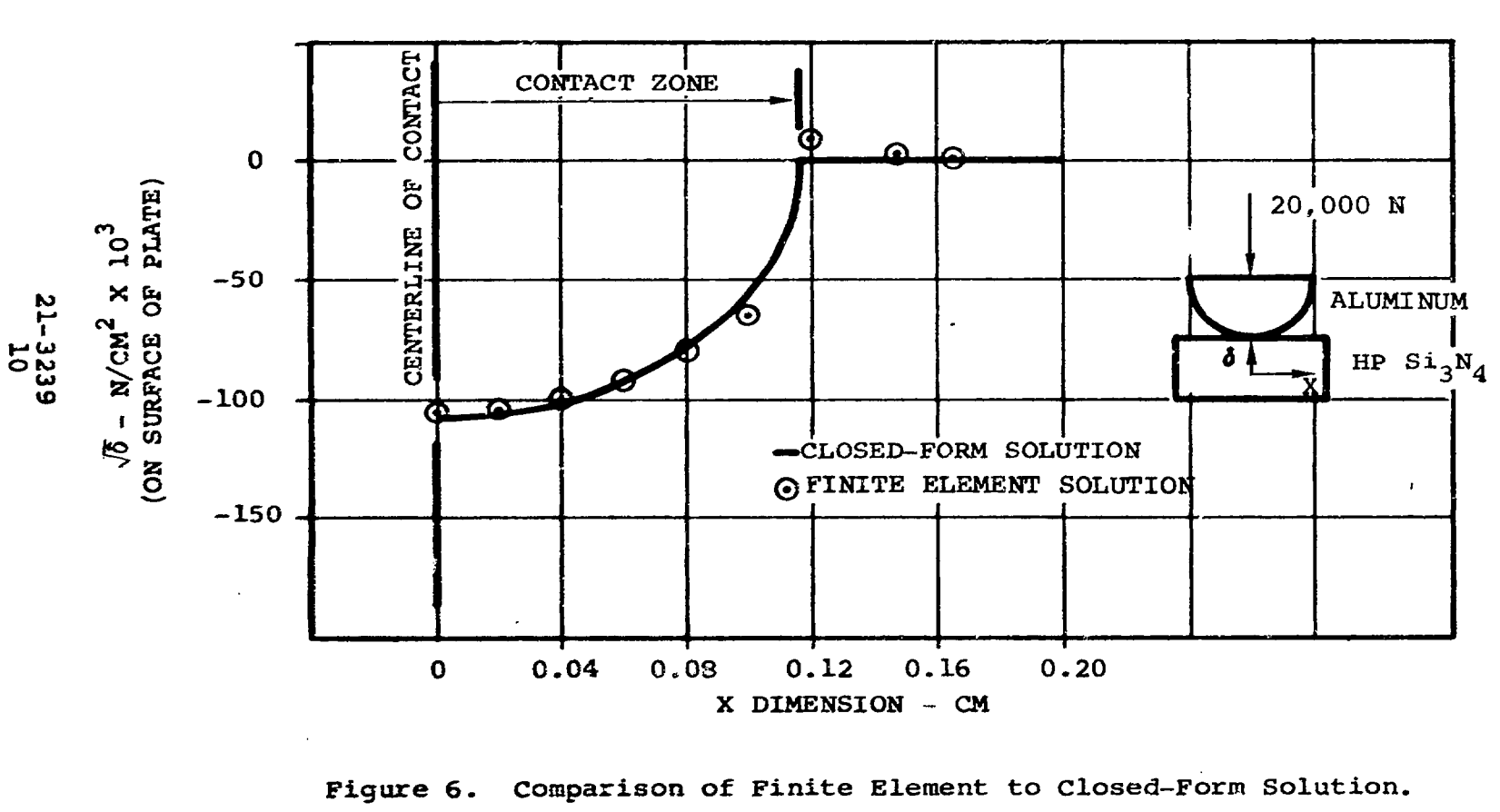

21-3239
10

Figure 6. Comparison of Finite Element to Closed-Form Solution.

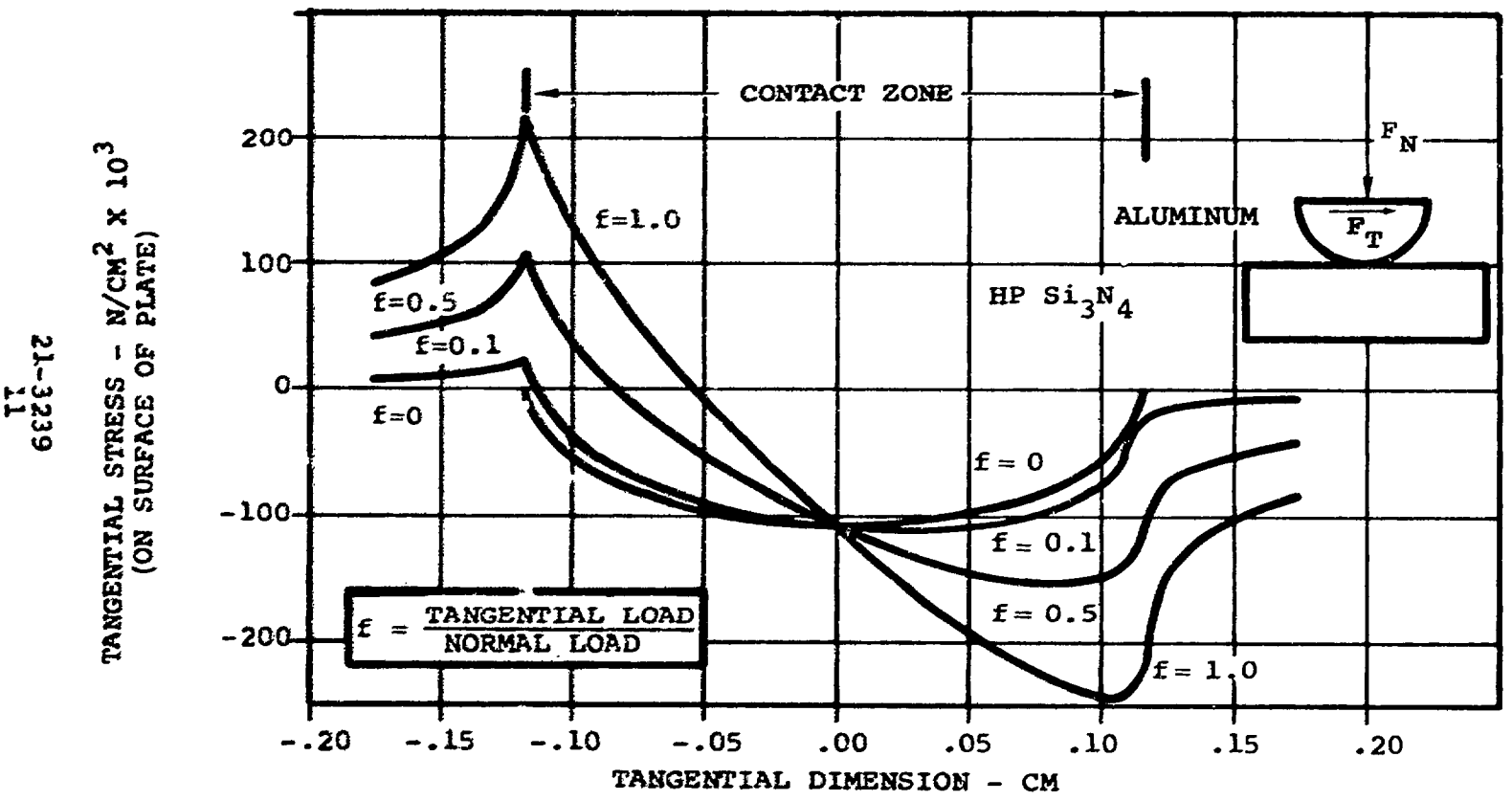

Figure 7. Contact Tangential Stresses for Different "f" Value.

and tangential loads. In the absence of tangential load, the stresses are compressive or non-existent along the surface. With the addition of tangential load, a tensile stress is generated at the edge of the contact zone. The tensile load increases as the tangential load is increased as long as there is no relative motion between the two bodies.

The peak tensile stress is very localized at the surface as well as at the edge of the contact zone. Figure 8 illustrates this stress peak at the surface. The peak tensile stress is considerably lower in magnitude, 0.001 centimeter below the surface.

Zoom modeling is required to determine the localized peak tensile stresses for contact interface problems using finite-element computer programs. Figure 9 compares a finite-element solution utilizing zoom modeling to a closed-form solution at the interface for a cylinder in contact with a flat plate for a normal/tangential load ratio equal to 3. Seven levels of zoom modeling were incorporated into the finite-element model to determine the peak tensile stress. The zoom finite-element mesh for determining the peak tensile stress is illustrated in Figure 10. Figures 9 and 11 show the localized nature of the peak tangential tensile stress.

2.2 Empirical Approach and Accomplishments

In addition to the analytical objectives of this program, specimen testing and data correlation are required to determine the failure mechanism and to formulate a failure theory for the complex state of stress in the contact interface zone. This verification testing was accomplished by simultaneously applying an axial load and a compressive normal contact load to the ceramic test specimens, Figure 12. The test fixture, Part No. STE-255277, is illustrated in Figure 13.

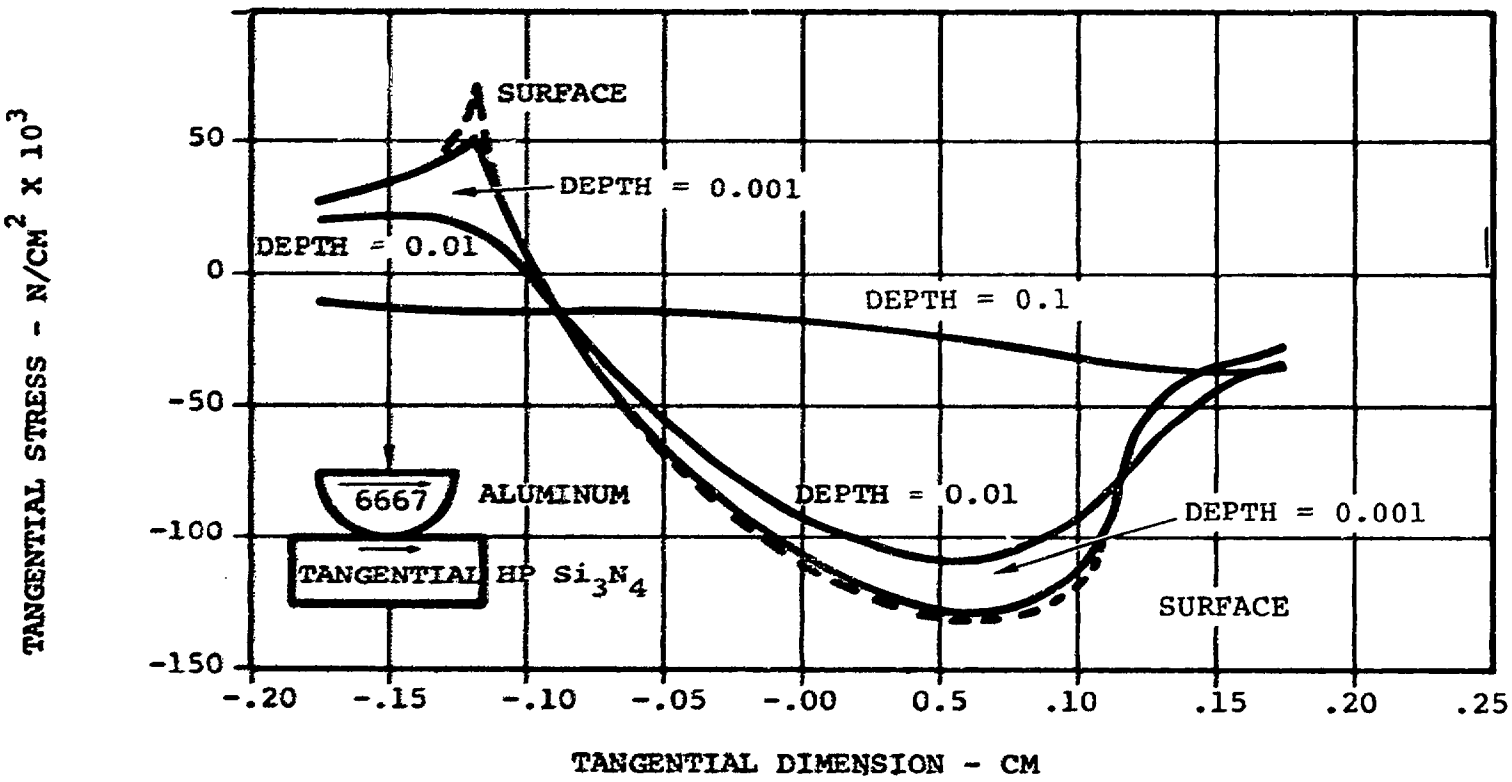

Figure 8. Contact Tangential Stresses Below the Surface.

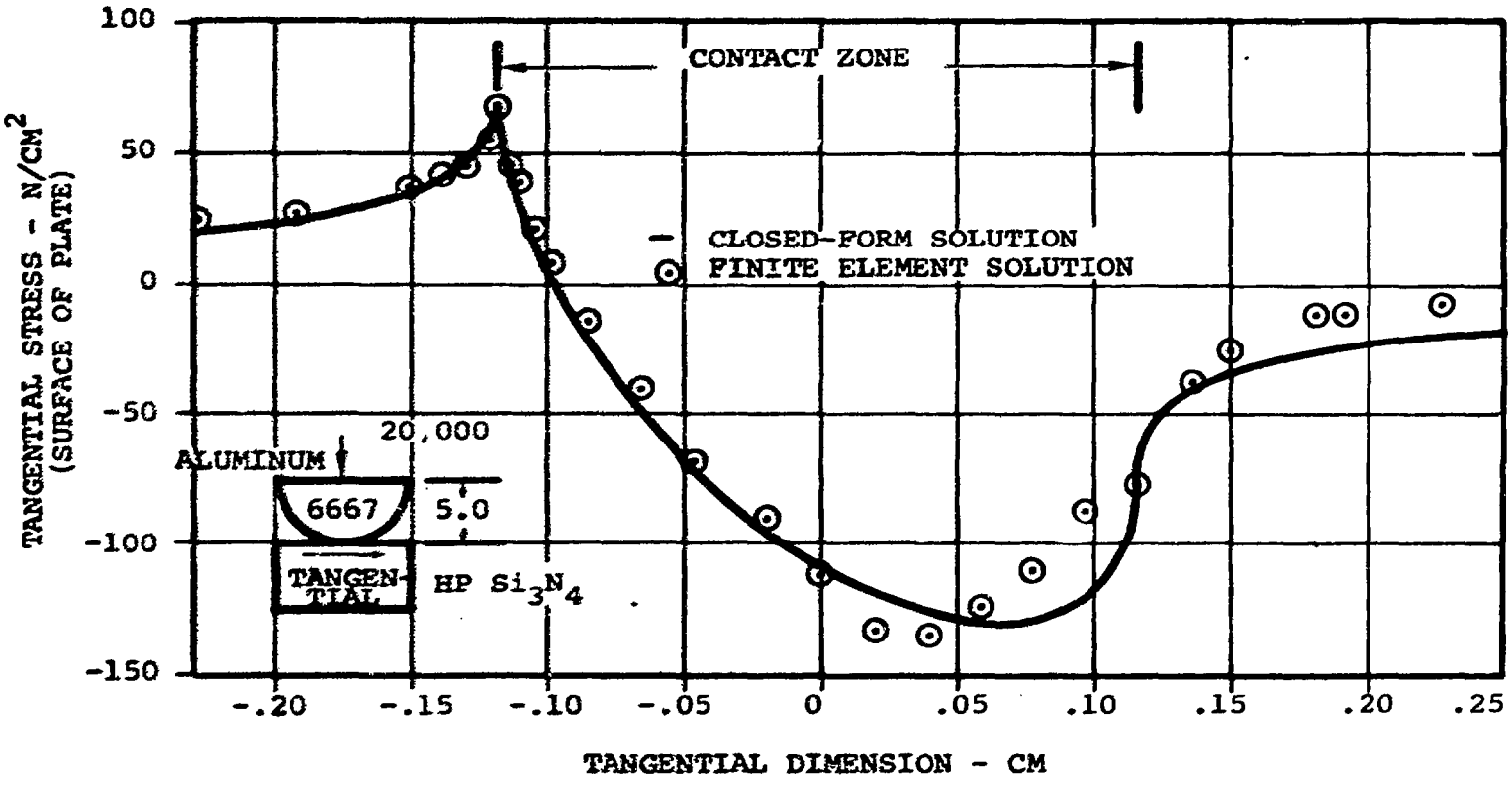

Figure 9. Comparison of Finite Element to Closed-Form Solution.

SCALE FACTOR = 1000

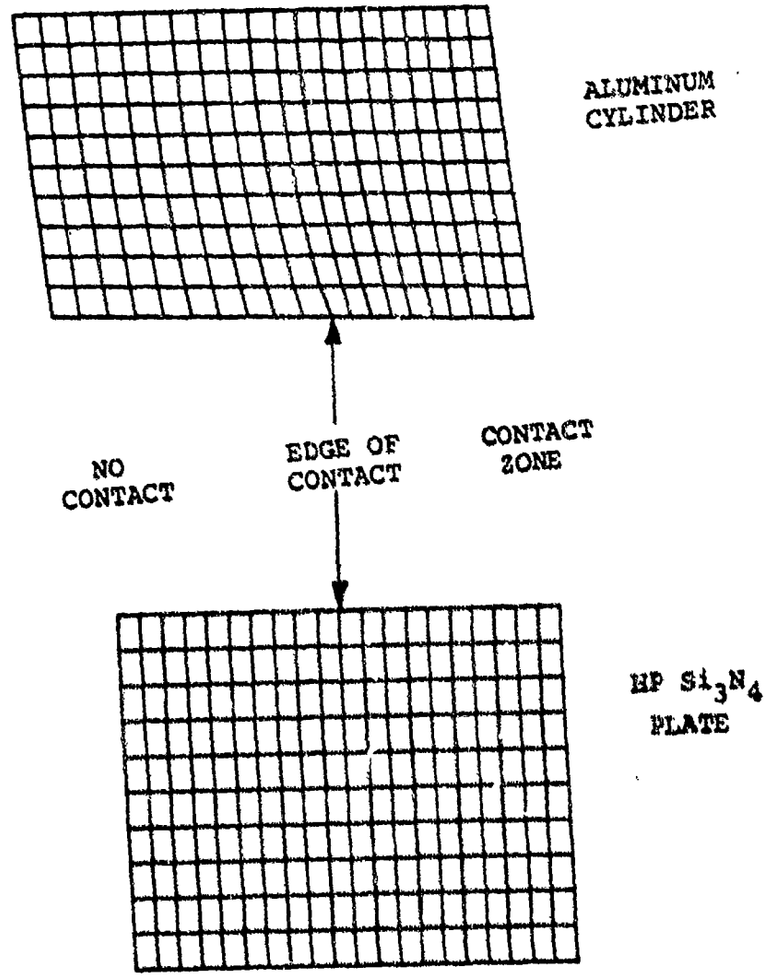

Figure 10. Refined Mesh Grid to Evaluate Peak Tensile Stress.

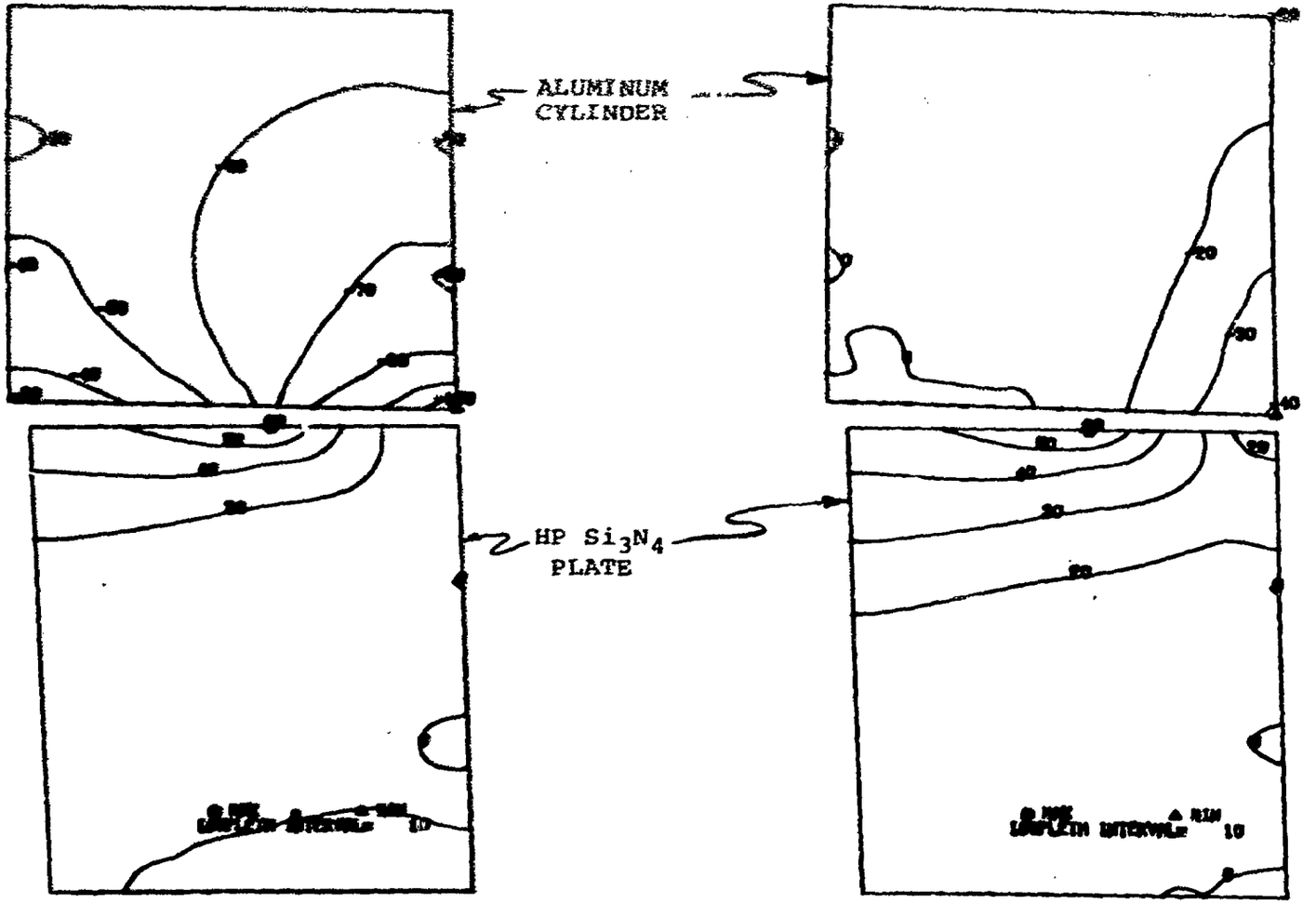

TANGENTIAL STRESS - $N/Cm^2 x10^3$

MAX. PRINCIPAL S RESS - $N/Cm^2 x10^3$

Figure 11. Finite-Element Stress Isopleths at Edge of Contact Zone.

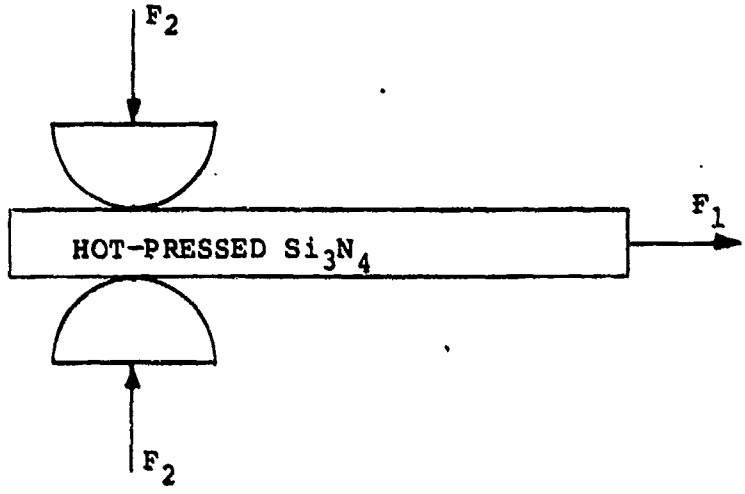

F_1 - Axial Load

F_2 - Compressive Normal Load

Figure 12. Ceramic Test Fixture Concept

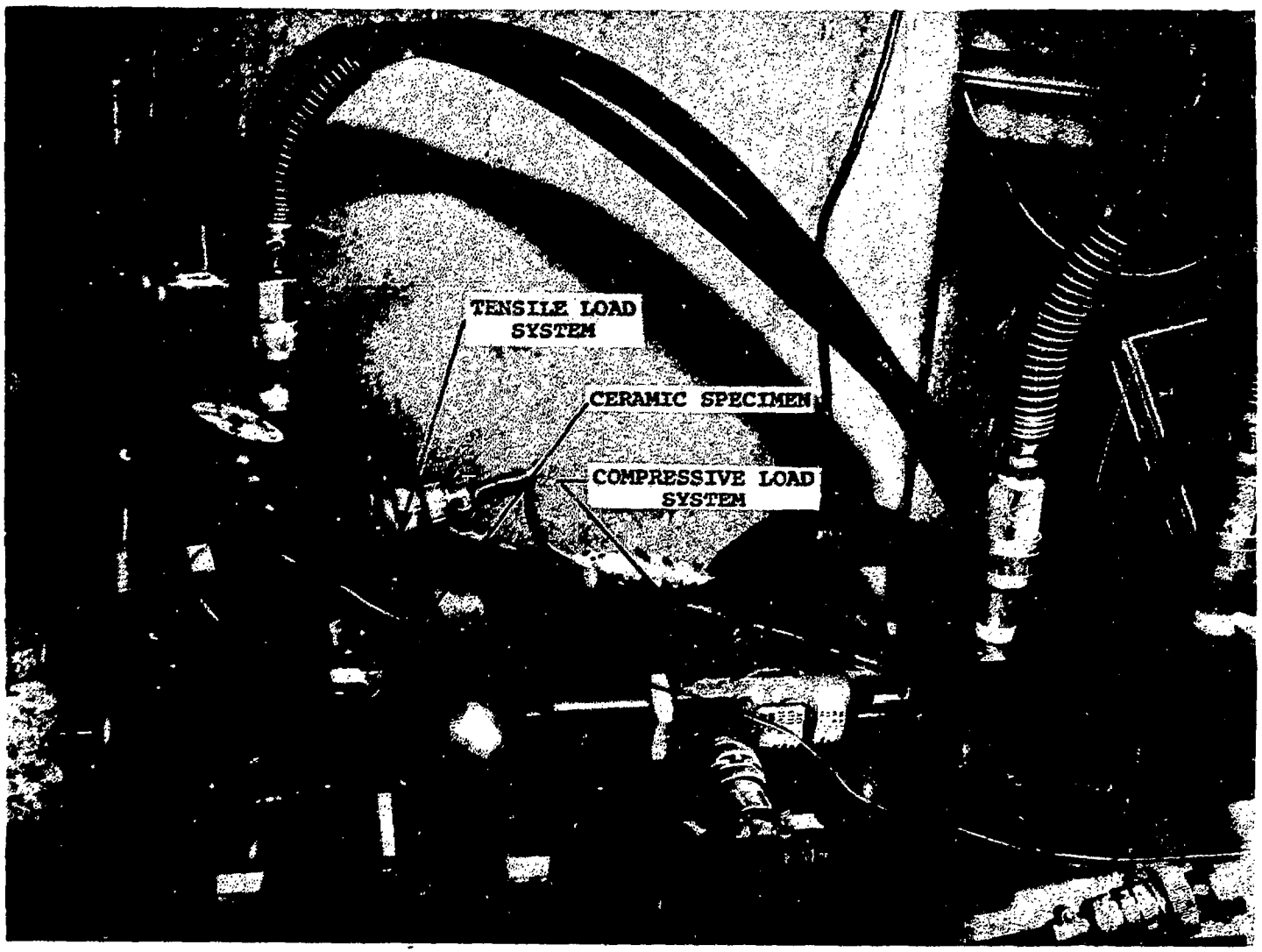

Figure 13. Ceramic Specimen Test Fixture.

Hot-pressed silicon nitride rectangular specimens (3 in. x 1/4 in. x 1/8 in.) were tested in contact with hardened 4340 steel cylinders. One of the cylinders was 2.0 inches in diameter and the other cylinder was 3.0 inches in diameter. The two cylinders were not identical to force the fractures to initiate on only one surface of the specimen. The stresses caused by the contact loads were approximately 25 percent higher on the surface in contact with the smaller cylinder.

The first seven samples were instrumented with strain gauges on both sides of the specimen to evaluate the amount of bending present during testing. All the fractures from this first set of samples initiated on the surface of the smaller diameter cylinder. Based on these results, it was deemed necessary to only instrument the side of the specimen in contact with the smaller diameter cylinder.

Testing was conducted by first placing a compressive contact load on the specimen. The axial load was then increased until slipping or fracture occurred. The compressive contact load, tensile axial load, and the axial strain on the specimen side near the smaller diameter cylinder were measured. Testing was also conducted with HS25 and platinum compliant material between the contacting bodies.

The coefficient of friction data exhibited good correlation with relatively small variations between test specimens. The average coefficient of friction between the hardened 4340 steel and the hot-pressed silicon nitride was 0.143. The measured data varied from 0.113 to 0.170. Figures 14 and 15 are two- and three-parameter Weibull plots of the coefficient of friction data, which illustrates its well-behaved nature. These data agree well with the published results for M50 tool steel on hot-pressed silicon nitride, Reference (3).

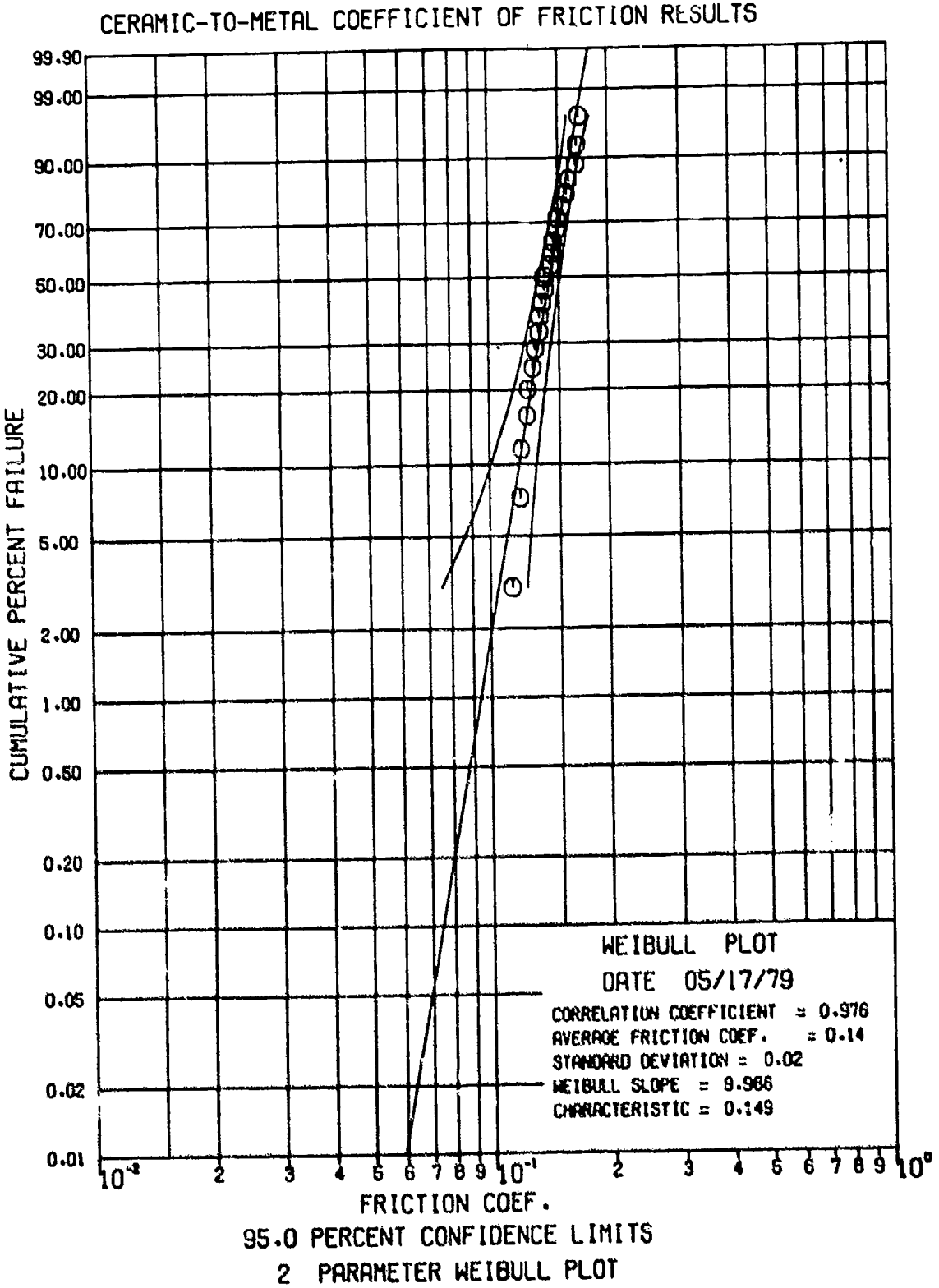
CERAMIC-TO-METAL COEFFICIENT OF FRICTION RESULTS
CUMULATIVE PERCENT FAILURE
99.90
99.00
90.00
70.00
50.00
30.00
20.00
10.00
5.00
2.00
1.00
0.50
0.20
0.10
0.05
0.02
0.01
WEIBULL PLOT
DATE 05/17/79
CORRELATION COEFFICIENT = 0.976
AVERAGE FRICTION COEF. = 0.14
STANDARD DEVIATION = 0.02
WEIBULL SLOPE = 9.966
CHARACTERISTIC = 0.149
FRICTION COEF.
95.0 PERCENT CONFIDENCE LIMITS
2 PARAMETER WEIBULL PLOT

Figure 14.

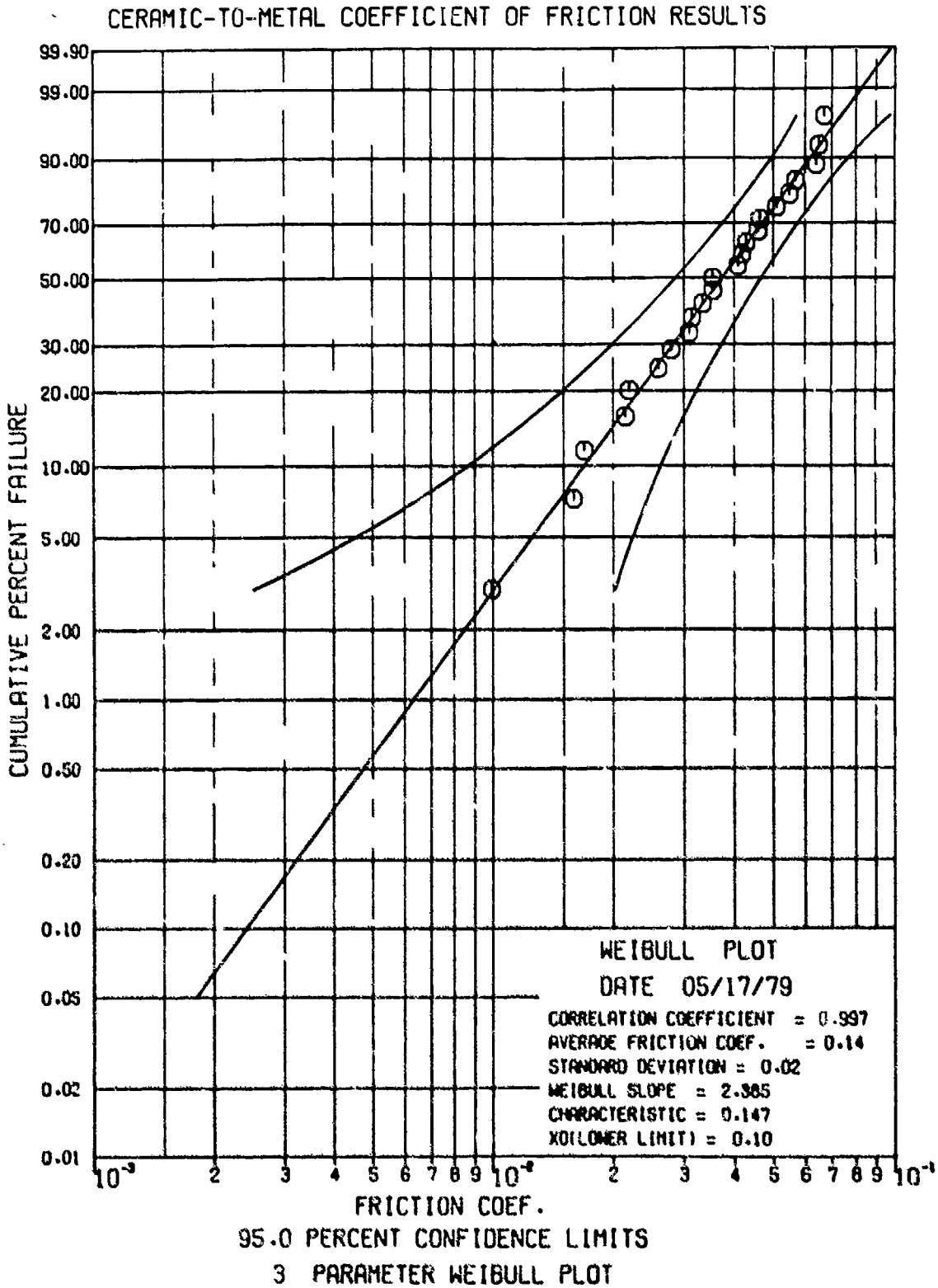
CERAMIC-TO-METAL COEFFICIENT OF FRICTION RESULTS
CUMULATIVE PERCENT FAILURE
99.90
99.00
90.00
70.00
50.00
30.00
20.00
10.00
5.00
2.00
1.00
0.50
0.20
0.10
0.05
0.02
0.01
WEIBULL PLOT
DATE 05/17/79
CORRELATION COEFFICIENT = 0.997
AVERAGE FRICTION COEF. = 0.14
STANDARD DEVIATION = 0.02
WEIBULL SLOPE = 2.385
CHARACTERISTIC = 0.147
X0(LOWER LIMIT) = 0.10
FRICTION COEF.
95.0 PERCENT CONFIDENCE LIMITS
3 PARAMETER WEIBULL PLOT

Figure 15.

Fracture data were accumulated from 1500 to 4000 pounds compressive load. In order to correlate and normalize all these data, the stresses due to the contact load were superimposed on the stresses caused by the axial tensile load. A classical solution, Reference (1), was used to calculate stresses in each specimen due to the contact loading. These calculated stresses were superimposed on the axial tensile stresses to determine the maximum tensile and maximum principal stresses at failure or when the specimen slipped.

The resulting stresses for both the fractures and slips are illustrated through the use of two- and three-parameter Weibull plots, Figures 16 and 17. The slip data are included in the statistical analysis as suspended items and the fracture data as failures. Based on the two-parameter Weibull plot, the characteristic strength is 94.5 KSI and the Weibull modulus is 4.2. Figure 18 compares the contact-fracture-strength results to four-point and three-point flexure data acquired from testing of specimens from the same billet of material. Under ideal test conditions, the resulting characteristic strength would be expected to be better than four-point flexure results and to be similar to three-point flexure results because the amount of stressed surface area during these tests is closer in size to the stressed surface area for three-point flexure tests. The scatter in the data can probably be attributed to specimen-to-specimen variations in surface finish in the interface zone, alignment of the specimen in the test fixture, and alignment of the contacting cylinders. As mentioned previously, the peak stresses are extremely localized, even more so than three-point flexure stresses. These localized stresses could possibly be affected by a different distribution of flaws than flexure stresses.

Another possibility for introducing errors into the fracture strength results are the stress calculations accounting for the contact loading. These two-dimensional stress calculations assume constant stress along the entire width of the test specimen. In actuality, these stresses are not constant. Even ignoring misalignment of

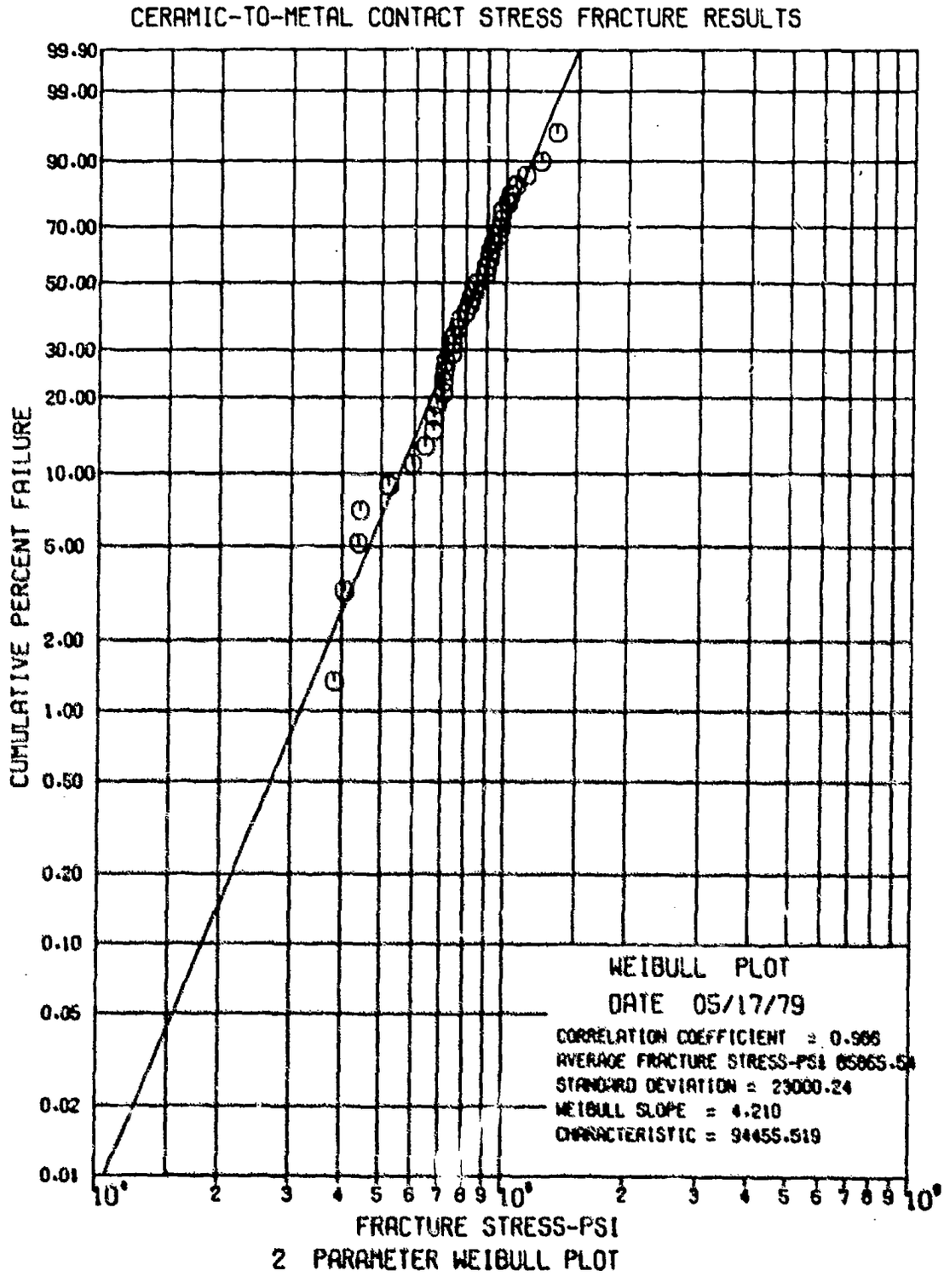
CERAMIC-TO-METAL CONTACT STRESS FRACTURE RESULTS
CUMULATIVE PERCENT FAILURE
99.90
99.00
90.00
70.00
50.00
30.00
20.00
10.00
5.00
2.00
1.00
0.50
0.20
0.10
0.05
0.02
0.01
WEIBULL PLOT
DATE 05/17/79
CORRELATION COEFFICIENT = 0.986
AVERAGE FRACTURE STRESS-PSI 85865.54
STANDARD DEVIATION = 23000.24
WEIBULL SLOPE = 4.210
CHARACTERISTIC = 94455.519
FRACTURE STRESS-PSI
2 PARAMETER WEIBULL PLOT

Figure 16.

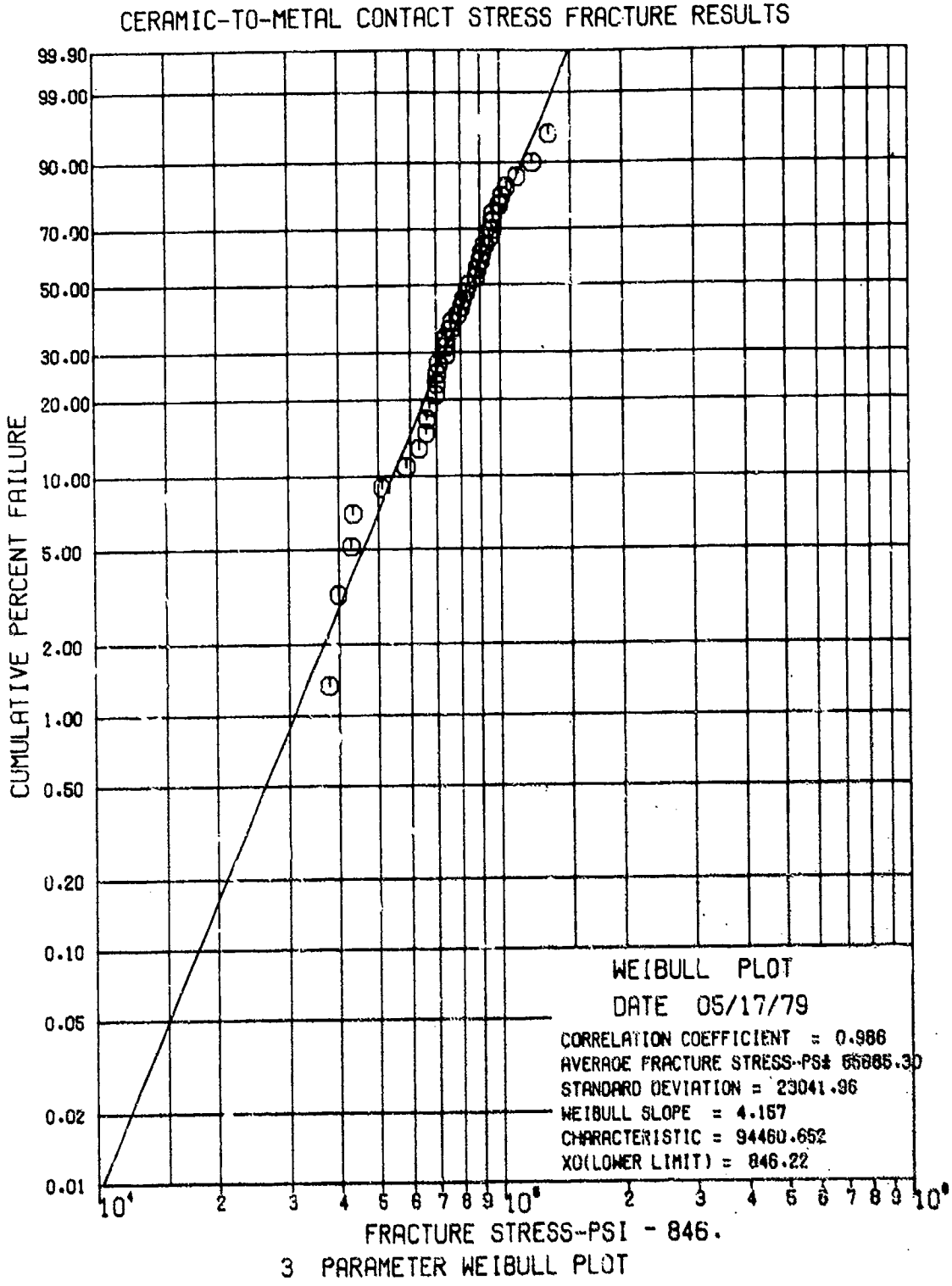
CERAMIC-TO-METAL CONTACT STRESS FRACTURE RESULTS
CUMULATIVE PERCENT FAILURE
99.90
99.00
90.00
70.00
50.00
30.00
20.00
10.00
5.00
2.00
1.00
0.50
0.20
0.10
0.05
0.02
0.01
10⁴ 2 3 4 5 6 7 8 9 10⁵ 2 3 4 5 6 7 8 9 10⁶
FRACTURE STRESS-PSI - 846.
3 PARAMETER WEIBULL PLOT
WEIBULL PLOT
DATE 05/17/79
CORRELATION COEFFICIENT = 0.986
AVERAGE FRACTURE STRESS-PSI 65885.30
STANDARD DEVIATION = 23041.96
WEIBULL SLOPE = 4.157
CHARACTERISTIC = 94460.652
XO(LOWER LIMIT) = 846.22

Figure 17.

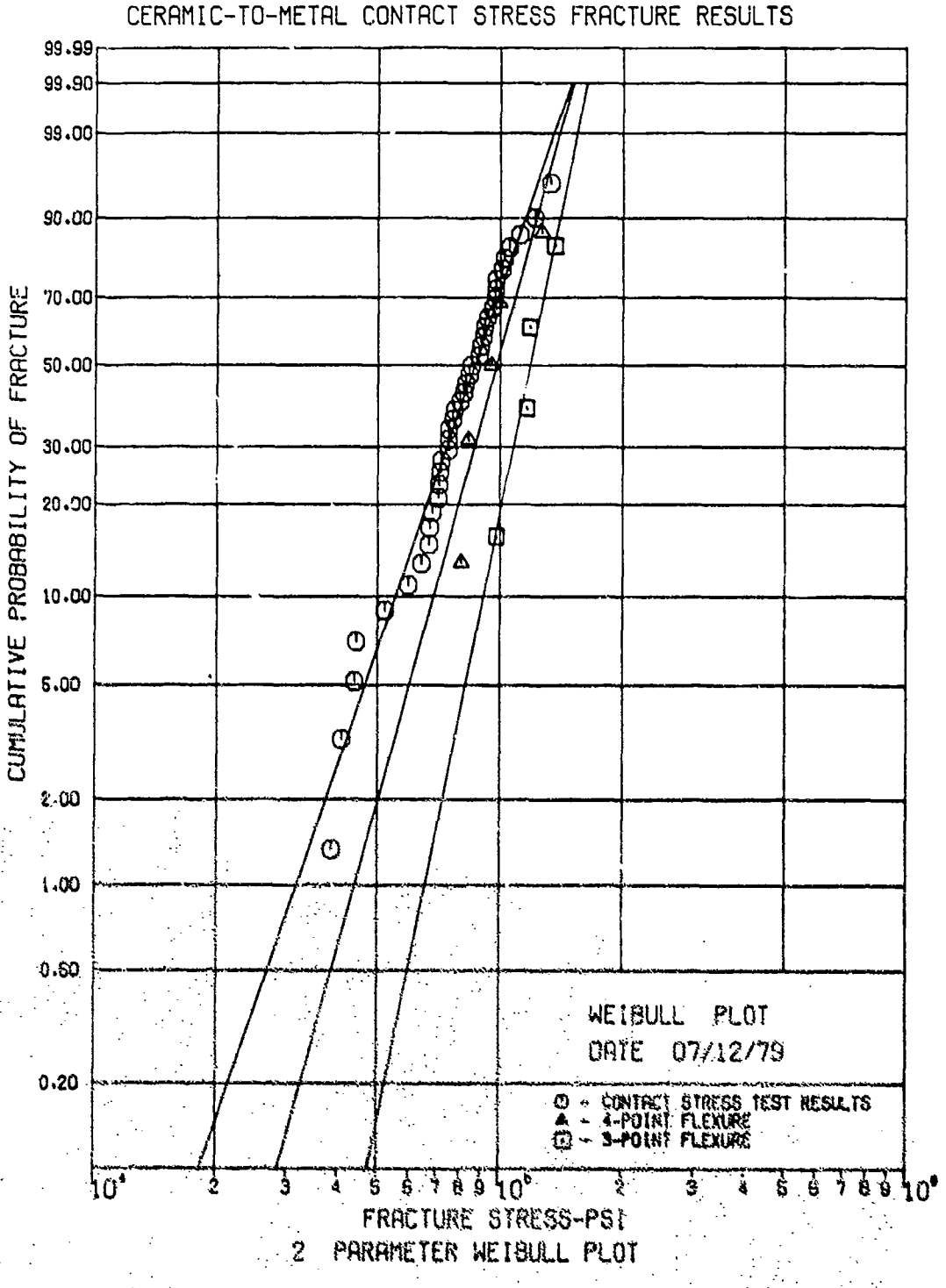
CERAMIC-TO-METAL CONTACT STRESS FRACTURE RESULTS
CUMULATIVE PROBABILITY OF FRACTURE
99.99
99.90
99.00
90.00
70.00
50.00
30.00
20.00
10.00
5.00
2.00
1.00
0.50
0.20
WEIBULL PLOT
DATE 07/12/79
⊙ - CONTACT STRESS TEST RESULTS
▲ - 4-POINT FLEXURE
⊡ - 3-POINT FLEXURE
10⁴ 2 3 4 5 6 7 8 9 10⁵ 2 3 4 5 6 7 8 9 10⁶
FRACTURE STRESS-PSI
2 PARAMETER WEIBULL PLOT

Figure 18.

the contacting cylinders, the state of stress at the edge of the specimen is plane stress and at the middle of the specimen is plane strain.

The test results are very reasonable and verify the maximum principal stress theory for failure prediction in brittle materials. All the fractures which have been examined to date indicate that the fractures originated on the surface at the edge of the contact zone, which is the location of maximum principal stress.

Testing has also been completed using HS25 and platinum compliant materials between the contacting surfaces.

Coefficient of friction data for these two compliant layers on hot-pressed silicon nitride is illustrated in Figure 19. The specimen could tolerate higher contact loads when the compliant layers were utilized. The higher loads were especially evident when the platinum layers were tested. However, the platinum was so ductile during testing that fracture strengths were impossible to measure. The platinum simply extruded until it was too thin to be an effective compliant medium. Consequently, in order to evaluate the life capabilities of "soft" compliant media similar to platinum, it is necessary to perform cyclic specimen tests.

Typical fracture surfaces are shown in Figure 20. Some of the fracture origins tended to be diffused and were not easily identified. Two such cases are shown in Figures 20(a) and 20(b). In other cases, Figure 20(c), the origin could be identified but was not as distinct as is typical of flexural test specimens of hot-pressed silicon nitride. This characteristic is probably related to the localized nature of the contact stresses, and the relatively small amount of stored elastic energy at fracture.

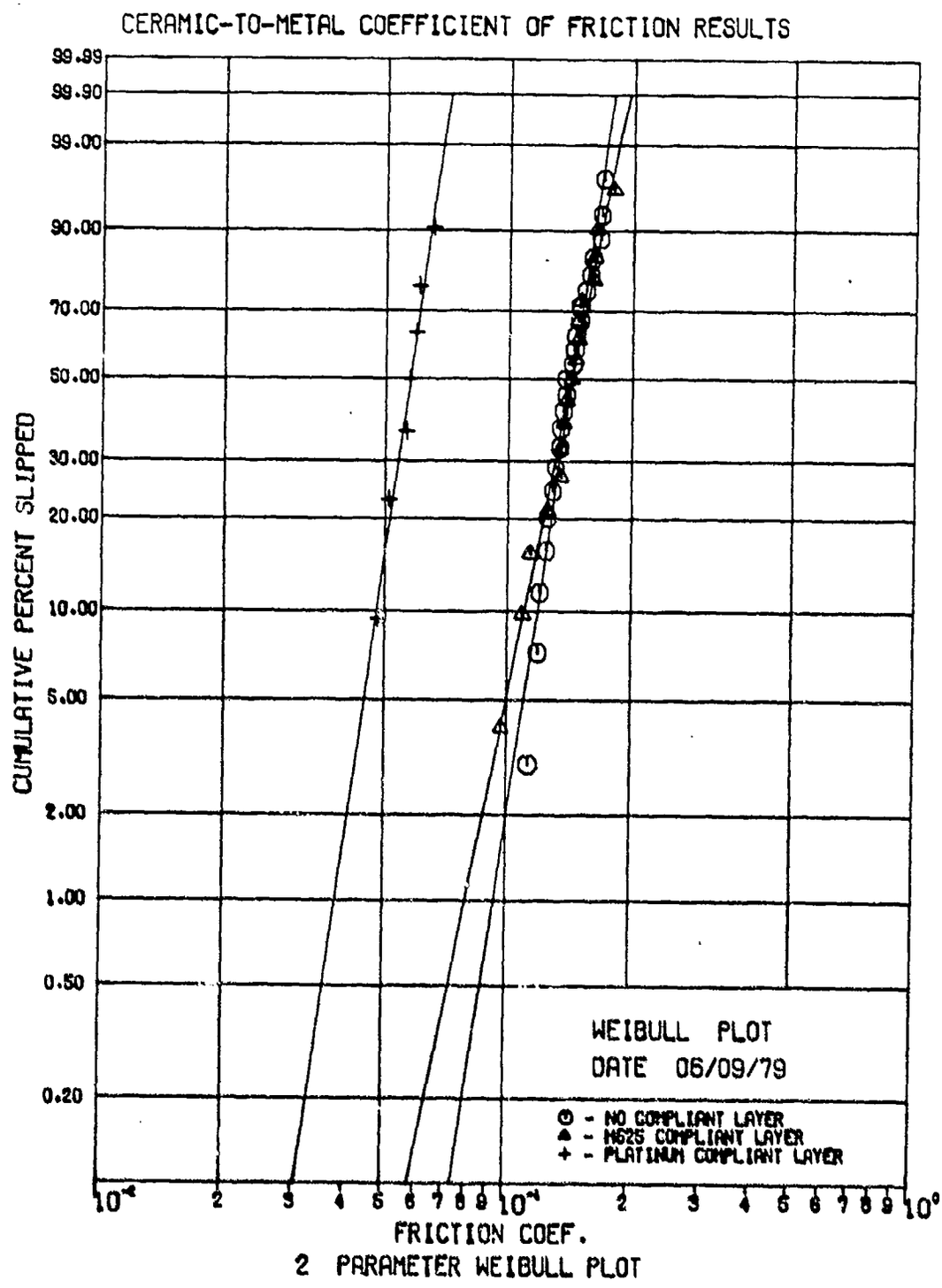
CERAMIC-TO-METAL COEFFICIENT OF FRICTION RESULTS
CUMULATIVE PERCENT SLIPPED
99.99
99.90
99.00
90.00
70.00
50.00
30.00
20.00
10.00
5.00
2.00
1.00
0.50
0.20
WEIBULL PLOT
DATE 06/09/79
⊙ - NO COMPLIANT LAYER
▲ - M625 COMPLIANT LAYER
+ - PLATINUM COMPLIANT LAYER
10⁻² 2 3 4 5 6 7 8 9 10⁻¹ 2 3 4 5 6 7 8 9 10⁰
FRICTION COEF.
2 PARAMETER WEIBULL PLOT

Figure 19.

(12X)

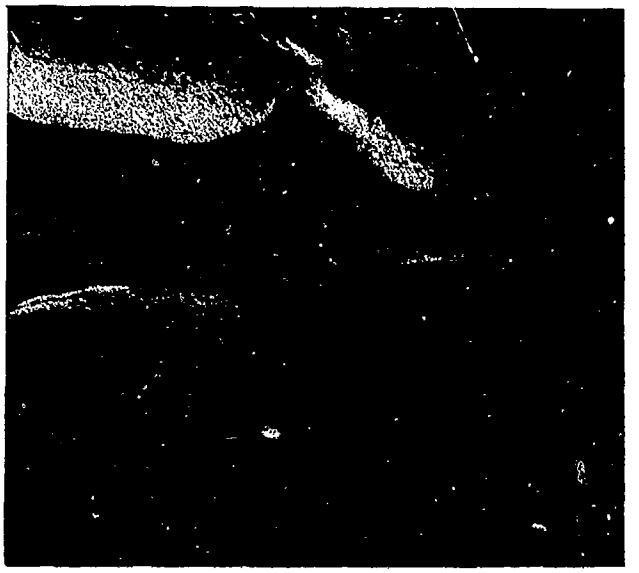

(22X)

(a) SPECIMEN NO. 18

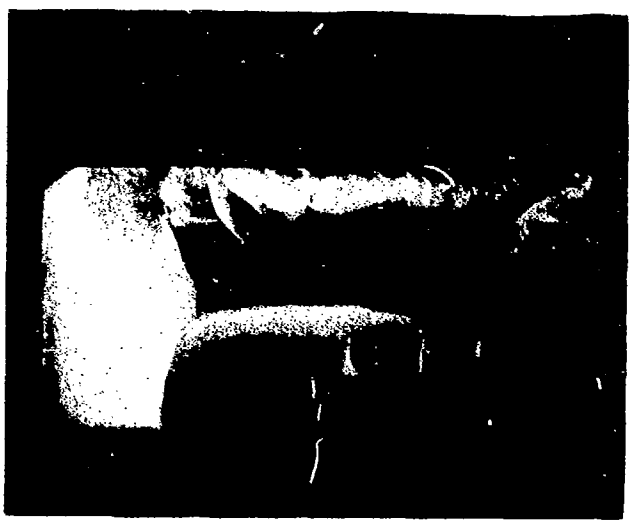

(12X)

(b) SPECIMEN NO. 14

Figure 20. SEM Photographs of Fracture Surfaces.

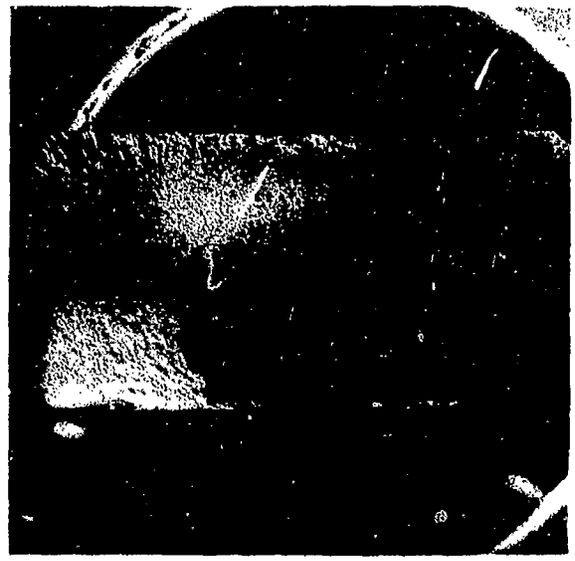

(12X)

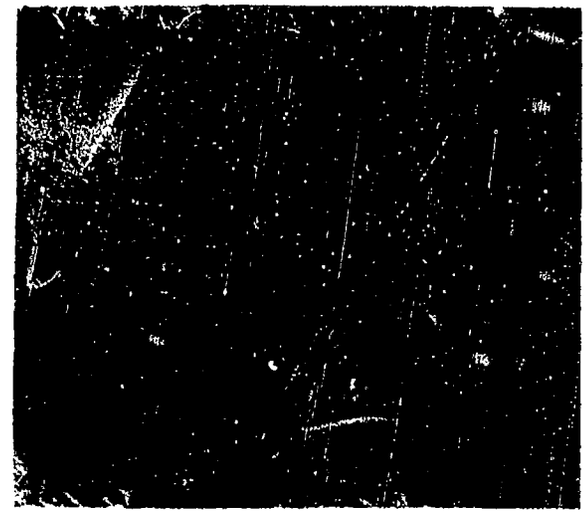

(22X)

(c) SPECIMEN NO. 20 (ARROW INDICATES FLAW ORIGIN AS DETERMINED UNDER LIGHT MICROSCOPE)

(12X)

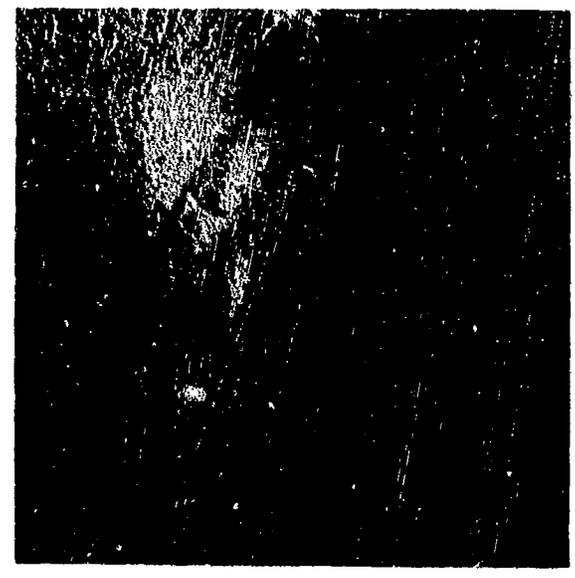

(25X)

(d) SPECIMEN NO. 8 (ARROW INDICATES HERTZIAN CONE CRACK)

Figure 20. (Contd.) SEM Photographs of Fracture Surfaces.

MP-68904

In several cases, there were indications that fracture initiated from a classical Hertzian cone crack. An example of fracture from a cone crack is shown in Figure 20(d). This type of crack is due to a contact stress localized at a point -- possibly due to a speck of dirt between the cylindrical contact and the specimen.

Another feature of the fracture surface which differed from specimen to specimen was the topography. Some specimens, Figures 20(c) and (d), had relatively smooth fracture surfaces while others, Figures 20(a) and (b), exhibited regions of considerable curvature. The exact reason for this difference is not known, but should be related to the contact stress distribution and the location of fracture initiation.

3.0 CONCLUSIONS

The following conclusions have been reached as a result of this contact-stress program.

(a) The finite-element approach using zoom modeling can be used to predict the state of stress in ceramic-to-metal contact interface zones.

(b) The probability of success for a ceramic-to-metal interface can be predicted using maximum principal stresses.

(c) Compliant media can increase the allowable contact loads which a ceramic can tolerate.

(d) More understanding of the necessary physical properties of a compliant media is required for a long-life application.

REFERENCES

1. Smith, J.O. and Chang Keng Liu, "Stresses Due to Tangential and Normal Loads on an Elastic Solid with Application to Some Contact Stress Problems," Journal of Applied Mechanics, Vol. 20, No. 2, June 1953, pp. 157-166.

2. Boresi, A.P., O.M. Sidebottom, F.B. Seely, J.O. Smith, Advanced Mechanics of Materials, Third Edition, pp. 581-627, John Wiley and Sons, 1978.

3. Chin, Y. and H. Dalal, "Lubricant Interaction with Silicon Nitride in Rolling Contact Applications," pp 589-607 in Ceramics For High Performance Applications, J. Burke, A. Gorum, and R. Katz editors, Brook Hill Publishing, 1974.